Effects of Mutual Coupling on Capacity of MIMO Vehicle-to-vehicle Systems

Alenka G. Zajić
Naval Research Laboratory, Washington, DC 20375 USA

***Abstract*— This paper proposes a three-dimensional (3-D) model for narrowband multiple-input multiple-output (MIMO) vehicle-to-vehicle (V-to-V) multipath fading channels that accounts for mutual coupling among both, transmit and receive antenna elements. This model is used to evaluate the effect of mutual coupling on the antenna element patterns and capacity of MIMO V-to-V systems in a variety of urban environments[1].**

I. Introduction

Several emerging wireless communication systems such as ad-hoc wireless networks, intelligent transportation systems, and relay-based cellular networks require direct transmission between mobile terminals. All these applications require robust, mobile, low-delay, and high reliability wireless communications. Development of these vehicle-to-vehicle (V-to-V) systems depends on a good characterization of outdoor V-to-V multipath fading channel. Since the characteristics of V-to-V channels significantly differ from those of conventional fixed-to-mobile (F-to-M) cellular radio channels [1], the new channel modeling techniques are required to avoid unnecessarily high error rates in the system. Akki and Haber [1] were the first to propose a two-dimensional (2-D) reference model for single-input single-output (SISO) V-to-V Rayleigh fading channels. Simulation models for SISO V-to-V channels have been reported in [2], [3]. The reference and simulation models for narrowband multiple-input multiple-output (MIMO) V-to-V channels have been proposed in [4]-[6], based on 2-D radio propagation. To more accurately model radio propagation in an urban V-to-V environment, the three-dimensional (3-D) reference and simulation models for narrowband and wideband MIMO V-to-V channels have been proposed in [7] and [8], respectively. Channel sounding measurements for wideband MIMO V-to-V channels in a variety of urban environments and the verification of 3-D model in [8] are reported in [9]. All these previously reported V-to-V models assume the wide spacings among transmit ($\mathrm{T_x}$) and receive ($\mathrm{R_x}$) antenna elements (i.e, several wavelengths) so that mutual coupling in the system can be neglected. However, in V-to-V communications, the robust compact antennas with reduced visual presence and aerodynamic drag are required. Hence, the $\mathrm{T_x}$ and $\mathrm{R_x}$ antennas with small inter-element spacings are desired. On the other hand, close antenna element spacing inevitably leads to mutual coupling [10]. The impact of mutual coupling on narroband and wideband MIMO systems in F-to-M propagation environments are reported in [11] - [14].

[1]This work has been supported by ONR.

In contrast, this paper analyzes the impact of mutual coupling on narrowband MIMO V-to-V systems. We first introduce a new 3-D model for narrowband MIMO V-to-V channels that accounts for mutual coupling among both $\mathrm{T_x}$ and $\mathrm{R_x}$ antenna elements. By combining the z-parameter representation of MIMO V-to-V $\mathrm{T_x}$ and $\mathrm{R_x}$ antenna subsystems with the h-parameter representation of the MIMO V-to-V channel in [8], we obtain our 3-D MIMO V-to-V channel model. The new 3-D model is used to evaluate the effect of mutual coupling on the $\mathrm{T_x}$ and $\mathrm{R_x}$ antenna patterns and capacity of MIMO V-to-V systems on urban surface street (USS) and Interstate highway (IH) road surfaces. First, we study the effect of mutual coupling on the dipole antenna patterns. The results show that mutual coupling noticeably changes the antenna pattern shape and radiated power. Furthermore, the results show that the presence of matching networks cannot change the antenna pattern to omnidirectional shape, i.e., the coupled dipole antenna pattern is not omnidirectional. The radiated power strongly depends on the angles of departure/arrival. Finally, the input-impedance and self-impedance matching networks improve radiated power of coupled antennas, while the characteristic impedance matching network is less effective. Then, we study the effect of mutual coupling on the capacity of MIMO V-to-V system. The results show that the MIMO V-to-V channel model without mutual coupling overestimates the available capacity for small antenna element spacings. This finding illustrates the importance of incorporating mutual coupling into propagation models. Furthermore, these results differ from those obtained in F-to-M channels, where the capacity with mutual coupling is larger than the capacity without mutual coupling for arbitrary antenna element spacings [11]. Finally, the results show that the capacities in USS and IH environments are similar, and hence independent of the propagation environment.

The remainder of this paper is organized as follows. Section II describes the MIMO V-to-V system with mutual coupling. Section III introduces the new 3-D model for narrowband MIMO V-to-V channels with mutual coupling and reviews the capacity of MIMO V-to-V system. Section IV analyzes the impact of mutual coupling on the antenna patterns and capacity of MIMO V-to-V systems. Finally, Section V provides some concluding remarks.

II. MIMO V-to-V System Model

This paper considers a narrowband MIMO V-to-V communication system with L_t transmit and L_r receive omnidirec-

tional antenna elements, as shown in Fig. 1. It is assumed that both the $\mathrm{T_x}$ and $\mathrm{R_x}$ are in motion and equipped with vertically-polarized half-wavelength electric dipole antenna elements. The radio propagation occurs in outdoor metropolitan environments that are characterized by 3-D non-isotropic scattering with either line-of-sight (LoS) or non-LoS conditions between the $\mathrm{T_x}$ and $\mathrm{R_x}$. We assume that the $\mathrm{T_x}$ and $\mathrm{R_x}$ antennas and the scatterers are in the far-field of one another.

A. Transmit and Receive Antenna Subsystems

The voltage sources V_{si} in Fig. 1, for $i = 1, \ldots, L_t$, have the source impedances Z_{si} and feed L_t antenna elements at the $\mathrm{T_x}$. The mutual coupling among the $\mathrm{T_x}$ antenna elements is characterized by an $L_t \times L_t$ impedance matrix $\mathbf{Z}_{TT}$, as shown in Fig. 1. The vector of voltages at the entrance of $\mathrm{T_x}$ coupling network, $\mathbf{V}_T$, is defined as

$$\mathbf{V}_T = \mathbf{V}_S - \mathbf{Z}_S \mathbf{i}_T, \tag{1}$$

where $\mathbf{V}_S = [V_{s1}, V_{s2}, \ldots, V_{sL_t}]^T$ is the vector of source voltages, $\mathbf{i}_T = [i_{t1}, i_{t2}, \ldots, i_{tL_t}]^T$ is the vector of $\mathrm{T_x}$ currents, $\mathbf{Z}_S$ is the diagonal matrix of source impedances, and $[\cdot]^T$ denotes transpose operation. Fig. 1 also shows the $\mathrm{R_x}$ that consists of L_r antenna elements and the load impedances Z_{Li}, for $i = 1, \ldots, L_r$. The mutual coupling among the $\mathrm{R_x}$ antenna elements is characterized by an $L_r \times L_r$ impedance matrix $\mathbf{Z}_{RR}$, as shown in Fig. 1. The vector of voltages at the exit of the $\mathrm{R_x}$ coupling network, $\mathbf{V}_R$, is defined as

$$\mathbf{V}_R = -\mathbf{Z}_L \mathbf{i}_R, \tag{2}$$

where $\mathbf{i}_R = [i_{r1}, i_{r2}, \ldots, i_{rL_r}]^T$ is the vector of $\mathrm{R_x}$ currents, and $\mathbf{Z}_L$ is the diagonal matrix of load impedances.

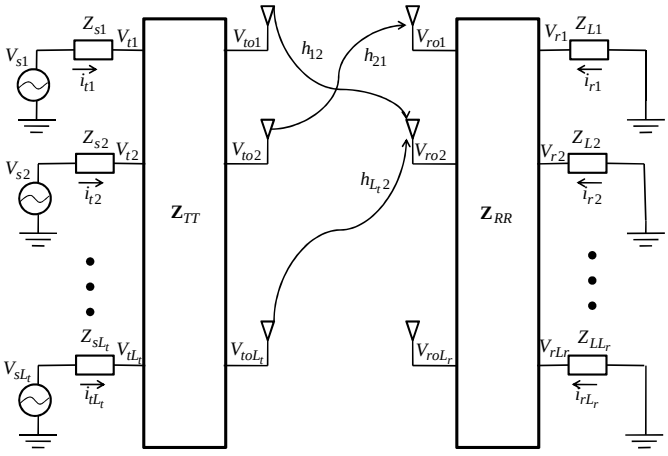

Fig. 1. Modeling of a MIMO V-to-V system using z- and h-parameters.

B. Impedance Matching Networks

The antenna pattern characteristics and the power collection capability of coupled antennas strongly depend on the impedance matching between the antenna inputs/outputs and the rest of communication network [11]. Therefore, the source and load impedances in Fig. 1 need to be selected carefully. Here, we briefly review four different impedance matching networks that are often used in the literature [11], [14].

The first matching network is the *characteristic impedance* matching network that has the $\mathrm{T_x}$ and $\mathrm{R_x}$ antenna elements terminated with the characteristic impedance Z_c, i.e., $Z_{si} = Z_c$ for $i = 1, \ldots, L_t$ and $Z_{Lk} = Z_c$, for $k = 1, \ldots, L_r$ [14]. The matching quality of the network depends on the difference between the antenna element impedance and the characteristic impedance. The second is the *self-impedance* matching network that has the $\mathrm{T_x}$ and $\mathrm{R_x}$ antenna elements terminated with the complex conjugated self-impedances, i.e., $Z_{si} = {Z_{TT}^{ii}}^*$ for $i = 1, \ldots, L_t$ and $Z_{Lk} = {Z_{RR}^{kk}}^*$, for $k = 1, \ldots, L_r$ [14], where $[\cdot]^*$ denotes the complex conjugate operation. This matching network facilitates the maximum power transfer between the antennas and communication electronics when there is no mutual coupling. However, when mutual coupling is present, the matching depends on the behavior of antenna mutual impedances. The third is the *input-impedance* matching network that has the $\mathrm{T_x}$ and $\mathrm{R_x}$ antenna elements terminated with the complex-conjugate input impedances, i.e., $Z_{si} = Z_{Ti}^{in\,*}$ for $i = 1, \ldots, L_t$ and $Z_{Lk} = {Z_{Rk}^{in}}^*$ for $k = 1, \ldots, L_r$ [14]. Similar to the self-impedance matching network, the input-impedance matching network has a single-branch matching. However, while the self-impedance matching network takes into account only the self-impedances of antenna elements, the input-impedance matching network takes into account both the self- and mutual impedances. Finally, the fourth is the *multi-port conjugate* matching network that, similar to the input-impedance matching network, takes into account the mutual coupling among the antenna elements [11]. Although this network offers both the zero return loss and zero correlation, its very narrow bandwidth and high complexity prevent practical implementation. Hence, in this paper, we will implement only the first three matching networks.

III. Modeling of V-to-V MIMO Channel with Mutual Coupling

A. MIMO V-to-V Channel without Mutual Coupling

The MIMO V-to-V channel without mutual coupling can be described by an $L_r \times L_t$ matrix $\mathbf{H}(t, \tau) = [h_{ij}(t, \tau)]_{L_r \times L_t}$ of the complex low-pass faded envelopes and can be defined as

$$\mathbf{V}_{Ro} = \mathbf{H}\ \mathbf{V}_{To}, \tag{3}$$

where $\mathbf{V}_{Ro} = [V_{ro1}, ..., V_{roL_r}]^T$ and $\mathbf{V}_{To} = [V_{to1}, ..., V_{toL_t}]^T$ are the vectors of the $\mathrm{R_x}$ and $\mathrm{T_x}$ open circuited voltages, respectively, as shown in Fig. 1. To characterize the complex faded envelopes of the matrix $\mathbf{H}$, we simplify the 3-D wideband MIMO V-to-V channel model in [8]. This model employs the two-cylinders geometry and constructs the complex faded envelope as a superposition of single-bounced transmit (SBT), single-bounced received (SBR), double-bounced (DB), and LoS rays, i.e,

$$h_{pq}(t) \quad = \quad h_{pq}^{SBT}(t) + h_{pq}^{SBR}(t) + h_{pq}^{DB}(t) + h_{pq}^{LoS}(t). \tag{4}$$

In this paper, we are interested in the spatial component of the complex faded envelope. Hence, without loss of generality, we

can set time t to zero. Than, the complex faded envelope in (4) simplifies to

$$h_{pq} = h_{pq}^{SBT} + h_{pq}^{SBR} + h_{pq}^{DB} + h_{pq}^{LoS}, \tag{5}$$

where

$$h_{pq}^{SBT} = \sqrt{\frac{\eta_T P_{pq}}{K+1}} \sum_{m=1}^{M} \frac{1}{\sqrt{M}} e^{-j\frac{2\pi}{\lambda}D} \tag{6}$$
$$e^{j\frac{2\pi}{\lambda}(0.5L_t+0.5-p)d_{Tx}\cos\alpha_T^{(m)}\cos\beta_T^{(m)}+j\phi_m}$$
$$e^{j\frac{2\pi}{\lambda}(0.5L_t+0.5-p)\left[d_{Ty}\sin\alpha_T^{(m)}\cos\beta_T^{(m)}+d_{Tz}\sin\beta_T^{(m)}\right]}$$
$$e^{j\frac{2\pi}{\lambda}(0.5L_r+0.5-q)d_R\cos\psi_R\left[\Delta_T\sin\theta_R\sin\alpha_T^{(m)}-\cos\theta_R\right]}$$

$$h_{pq}^{SBR} = \sqrt{\frac{\eta_R P_{pq}}{K+1}} \sum_{n=1}^{N} \frac{1}{\sqrt{N}} e^{-j\frac{2\pi}{\lambda}D} \tag{7}$$
$$e^{j\frac{2\pi}{\lambda}(0.5L_r+0.5-q)d_{Rx}\cos\alpha_R^{(n)}\cos\beta_R^{(n)}+j\phi_n}$$
$$e^{j\frac{2\pi}{\lambda}(0.5L_r+0.5-q)\left[d_{Ry}\sin\alpha_R^{(n)}\cos\beta_R^{(n)}+d_{Rz}\sin\beta_R^{(n)}\right]}$$
$$e^{j\frac{2\pi}{\lambda}(0.5L_t+0.5-p)d_T\cos\psi_T\left[\Delta_R\sin\theta_T\sin\alpha_R^{(n)}+\cos\theta_T\right]}$$

$$h_{pq}^{DB} = \sqrt{\frac{\eta_{TR} P_{pq}}{K+1}} \sum_{m=1}^{M}\sum_{n=1}^{N} \frac{1}{\sqrt{MN}} \tag{8}$$
$$e^{j\frac{2\pi}{\lambda}(0.5L_t+0.5-p)d_{Tx}\cos\alpha_T^{(m)}\cos\beta_T^{(m)}}$$
$$e^{j\frac{2\pi}{\lambda}(0.5L_t+0.5-p)\left[d_{Ty}\sin\alpha_T^{(m)}\cos\beta_T^{(m)}+d_{Tz}\sin\beta_T^{(m)}\right]}$$
$$e^{-j\frac{2\pi}{\lambda}D+j\phi_{m,n}+\frac{2\pi}{\lambda}(0.5L_r+0.5-q)d_{Rz}\sin\beta_R^{(n)}}$$
$$e^{j\frac{2\pi}{\lambda}(0.5L_r+0.5-q)\left[d_{Rx}\cos\alpha_R^{(n)}\cos\beta_R^{(n)}+d_{Ry}\sin\alpha_R^{(n)}\cos\beta_R^{(n)}\right]}$$

$$h_{pq}^{LoS} = \sqrt{\frac{KP_{pq}}{K+1}} e^{-j\frac{2\pi}{\lambda}D+j\frac{2\pi}{\lambda}(0.5L_t+0.5-p)d_T\cos\theta_T\cos\psi_T}$$
$$e^{j\frac{2\pi}{\lambda}(0.5L_r+0.5-q)d_R\cos\psi_R\cos(\pi-\theta_R)}, \tag{9}$$

In (6)–(9), K denotes the Rice factor (ratio of LoS to scatter received power), λ denotes the carrier wavelength, P_{pq} is the power transmitted through the sub-channel between pth transmit and qth receive antennas, D is the distance between the $\mathrm{T_x}$ and $\mathrm{R_x}$, and the parameters p and q take values from the sets $p \in \{1,\ldots,L_t\}$ and $q \in \{1,\ldots,L_r\}$, respectively. The parameters η_T, η_R, and η_{TR} specify how much the single- and double-bounced rays contribute in the total averaged power, i.e., these parameters satisfy $\eta_T + \eta_R + \eta_{TR} = 1$. The parameters M and N denote number of fixed scatterers lying on the cylindric surfaces with radii R_t and R_r around the $\mathrm{T_x}$ and $\mathrm{R_x}$, respectively. The spacings between antenna elements at the $\mathrm{T_x}$ and $\mathrm{R_x}$ are denoted by d_T and d_R, respectively. Angles θ_T and θ_R describe the orientation of the $\mathrm{T_x}$ and $\mathrm{R_x}$ antenna array in the azimuthal plane. Similarly, angles ψ_T and ψ_R describe the elevation of the $\mathrm{T_x}$'s and the $\mathrm{R_x}$'s antenna array relative to the azimuthal plane, respectively. Finally, $d_{Tz} = d_T\sin\psi_T$, $d_{Tx} = d_T\cos\psi_T\cos\theta_T$, $d_{Ty} = d_T\cos\psi_T\sin\theta_T$, $d_{Rz} = d_R\sin\psi_R$, $d_{Rx} = d_R\cos\psi_R\cos\theta_R$, $d_{Ry} = d_R\cos\psi_R\sin\theta_R$, and $\Delta_{T/R} = R_{t/r}/D$.

This model assumes that the angles of departure ($\alpha_T^{(m)}$ and $\beta_T^{(m)}$) and the angles of arrival ($\alpha_R^{(n)}$ and $\beta_R^{(n)}$) are independent random variables. Furthermore, it assumes that the phases ϕ_m, ϕ_n, and $\phi_{m,n}$ are random variables uniformly distributed on the interval $[-\pi,\pi)$ and independent from the angles of departure and the angles of arrival. The azimuth angles of departure and arrival (α_T and α_R) are characterized by the von Mises pdf as $f(\alpha_T) = \exp\left[k_T\cos(\alpha_T-\mu_T)\right]/2\pi I_0(k_T)$ and $f(\alpha_R) = \exp\left[k_R\cos(\alpha_R-\mu_R)\right]/2\pi I_0(k_R)$, respectively, where $\alpha_{T/R} \in [-\pi,\pi)$, $I_0(\,\cdot\,)$ is the zeroth-order modified Bessel function of the first kind, $\mu_{T/R} \in [-\pi,\pi)$ are the mean angles at which the scatterers are distributed in the azimuthal plane, and $k_{T/R}$ control the spread of scatterers around the $\mathrm{T_x}$ and $\mathrm{R_x}$, respectively. Finally, the elevation angles of departure and arrival (β_T and β_R) are characterized by the pdfs $f(\beta_T) = \pi\cos(\pi\beta_T/(2\beta_{T_m}))/(4|\beta_{T_m}|)$ and $f(\beta_R) = \pi\cos(\pi\beta_R/(2\beta_{R_m}))/(4|\beta_{R_m}|)$, respectively, where β_{T_m} and β_{R_m} are the maximum elevation angles around the $\mathrm{T_x}$ and $\mathrm{R_x}$, respectively.

B. MIMO V-to-V Channel with Mutual Coupling

To include effects of mutual coupling into MIMO V-to-V channel matrix $\mathbf{H}$, we introduce an $L_r \times L_t$ channel matrix $\mathbf{H}^c$ and define as

$$\mathbf{V}_R = \mathbf{H}^c\ \mathbf{V}_S. \tag{10}$$

To evaluate the channel matrix $\mathbf{H}^c$, we model the MIMO V-to-V system in Fig. 1 as a multi-port network with the voltages and currents related as follows

$$\begin{bmatrix} \mathbf{V}_R \\ \mathbf{V}_T \end{bmatrix} = \begin{bmatrix} \mathbf{Z}_{RR} & \mathbf{Z}_{RT} \\ \mathbf{Z}_{TR} & \mathbf{Z}_{TT} \end{bmatrix} \begin{bmatrix} \mathbf{i}_R \\ \mathbf{i}_T \end{bmatrix}. \tag{11}$$

The sub-block matrices $\mathbf{Z}_{TT}$ and $\mathbf{Z}_{RR}$ in (11) denote the mutual coupling among $\mathrm{T_x}$ and $\mathrm{R_x}$ antenna elements, respectively, the sub-block matrix $\mathbf{Z}_{RT}$ denotes the propagation from the $\mathrm{T_x}$ to $\mathrm{R_x}$, and the sub-block matrix $\mathbf{Z}_{TR}$ denotes the propagation from the $\mathrm{R_x}$ to $\mathrm{T_x}$. In the further analysis, we assume that the backscattering from the $\mathrm{R_x}$ to $\mathrm{T_x}$ is negligible, i.e., $\mathbf{Z}_{TR} = 0$. By substituting (1) and (2) into (11), and by solving the system of equations, the channel matrix $\mathbf{H}^c$ becomes

$$\mathbf{H}^c = \frac{\mathbf{Z}_L}{(\mathbf{Z}_L+\mathbf{Z}_{RR})}\mathbf{H}\frac{\mathbf{Z}_{TT}}{(\mathbf{Z}_S+\mathbf{Z}_{TT})} = \mathbf{Z}_R\mathbf{H}\mathbf{Z}_T, \tag{12}$$

where $\mathbf{Z}_R = \mathbf{Z}_L(\mathbf{Z}_L+\mathbf{Z}_{RR})^{-1}$ and $\mathbf{Z}_T = \mathbf{Z}_{TT}(\mathbf{Z}_S+\mathbf{Z}_{TT})^{-1}$.

C. Capacity of MIMO V-to-V Channel with Mutual Coupling

The instantaneous channel capacity (in $\mathrm{bit/s/Hz}$) of a stochastic MIMO V-to-V channel *with* mutual coupling, under an average transmit power constraint is [5]

$$C_c = \log_2\det\left(\mathbf{I}_{L_r} + \frac{\rho}{L_t}\mathbf{H}^c\mathbf{H}^{c^H}\right), \tag{13}$$

where it is assumed that $L_t \geq L_r$, the $\mathrm{T_x}$ has no channel knowledge, and the $\mathrm{R_x}$ has perfect channel knowledge. In (13), $\mathbf{H}^c = [h_{ij}^c]_{L_r\times L_t}$ is the $L_r \times L_t$ matrix defined in (10), $(\,\cdot\,)^H$ denotes the transpose conjugate operation, $\det(\,\cdot\,)$ denotes the matrix determinant, $\mathbf{I}_{L_r}$ is the $L_r \times L_r$ identity matrix, and ρ is the average signal-to-noise ratio (SNR). Similarly, the instantaneous channel capacity (in $\mathrm{bit/s/Hz}$) of a stochastic

MIMO V-to-V channel *without* mutual coupling, under an average transmit power constraint is

$$C \quad = \quad \log_2 \det \left(\mathbf{I}_{L_r} + \frac{\rho}{L_t} \mathbf{H}\mathbf{H}^H \right), \qquad (14)$$

where $\mathbf{H} = [h_{ij}]_{L_r \times L_t}$ is the $L_r \times L_t$ matrix defined in (3).

IV. Numerical Results

This section analyzes the impact of mutual coupling on the $\mathrm{T_x}$ and $\mathrm{R_x}$ antenna patterns and capacity of MIMO V-to-V systems. In all simulations, we analyze a 2×2 MIMO V-to-V system. The vertically-polarized half-wavelength ($\lambda/2$) electric dipole antennas with radii $\lambda/600$ are selected as the $\mathrm{T_x}$ and $\mathrm{R_x}$ antenna elements, where $\lambda = 123.3$ mm. The antenna dipoles are modelled using AWAS, the method-of-moments based software [15]. The Z_c is set to $50\ \Omega$, the assumption commonly used in practice.

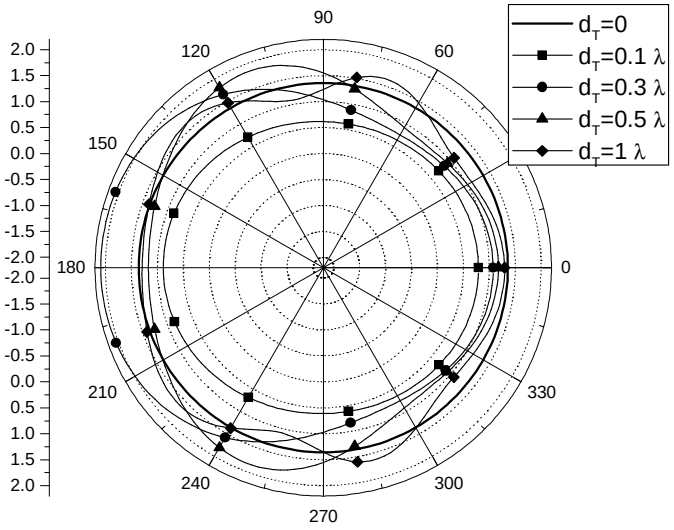

Fig. 2. The coupled dipole antenna pattern in the azimuthal plane as a function of antenna element spacings. The second dipole antenna is terminated with $Z_c = 50\Omega$.

To illustrate the effect of mutual coupling on the dipole antenna pattern, Fig. 2 plots the radiation pattern of one of the $\mathrm{T_x}$ dipoles for several different antenna spacings, i.e., $d_T \in \{0, 0.1\lambda, 0.3\lambda, 0.5\lambda, 1\lambda\}$. The other $\mathrm{T_x}$ dipole is terminated with the characteristic impedance Z_c. The $\mathrm{R_x}$ antenna elements have negligible effect on the $\mathrm{T_x}$ antenna patterns because they are in the far-filed of the $\mathrm{T_x}$ antenna elements. From Fig. 2, we can observe that the isolated dipole antenna (i.e., $d_T = 0$) has the omnidirectional pattern. When the second antenna element is introduced and their spacing is very small (i.e., $d_T = 0.1\lambda$), the pattern remains omni-directional, but the radiated power is significantly reduced. For the distances $0.3\lambda - 0.5\lambda$, mutual coupling noticeably changes the antenna pattern shape and the radiated power. The antenna pattern does not remain omnidirectional, and the radiated power becomes a function of the angles of departure and arrival. Finally, for antenna spacings greater or equal to 1λ, the mutual coupling has less impact on the antenna radiation and the pattern resembles that of the isolated dipole antenna.

To characterize the influence of different matching networks on the dipole antenna pattern, Fig. 3 plots the radiation pattern of one of the $\mathrm{T_x}$ dipoles, when all antenna elements are terminated with the characteristic, self-, and input-impedance matching networks, respectively. For the reference, we also plot the antenna pattern of an isolated dipole antenna. The coupling impedance matrices $\mathbf{Z}_{TT}$ and $\mathbf{Z}_{RR}$ are obtained using AWAS, the input impedances are calculated using the results in [14], and the spacing between antenna elements is $d_T = 0.3\lambda$. Fig. 3 shows that mutual coupling noticeably changes the antenna pattern shape and radiated power. Furthermore, the presence of matching networks cannot change the antenna pattern to omnidirectional shape, i.e., the coupled dipole antenna pattern is not omnidirectional and the radiated power strongly depends on the angles of departure/arrival. Finally, Fig. 3 shows that the input-impedance and self-impedance matching networks significantly improve the radiated power of coupled antennas, while the characteristic impedance matching network is less effective.

To analyze the capacity of MIMO V-to-V systems, Figs. 4 and 5 compare the mean capacities of MIMO V-to-V channels in USS and IH environments, respectively. The coupled $\mathrm{T_x}$ and $\mathrm{R_x}$ antennas are terminated with the characteristic, self-, and input-impedance matching networks, respectively. Fig. 4 assumes the 3-D non-isotropic radio propagation ($k_T = k_R = 3$, $\beta_{T_m} = \beta_{R_m} = 10^\circ$) in the USS environments ($\eta_T = \eta_R = 0.05$, $\eta_{TR} = 0.9$). Note that in USS environments, the double-bounced rays bear more energy than the single-bounced rays [9]. The curves are obtained with the parameters

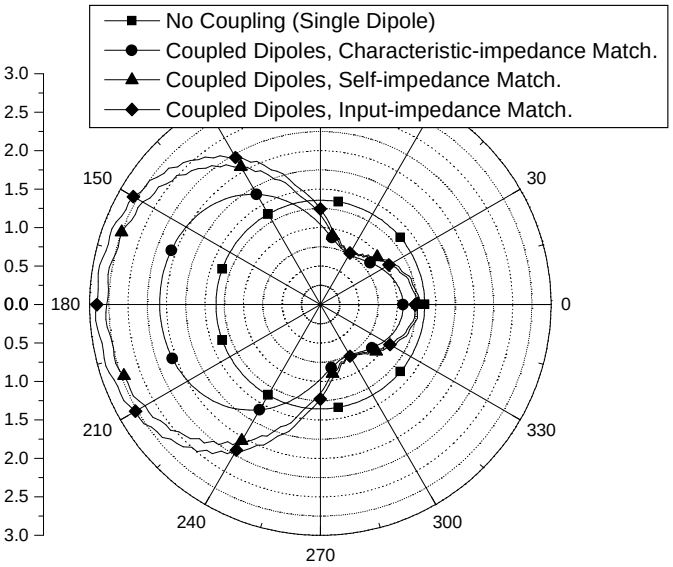

Fig. 3. The coupled dipole antenna patterns in the azimuthal plane, terminated with the characteristic, self-, and input-impedance matching network.

$\mu_T = \mu_R = 0^\circ$ and $K = 0$. Furthermore, we use $M = 50$ and $N = 50$ fixed scatterers. The distance between the $\mathrm{T_x}$ and $\mathrm{R_x}$ is $D = 300$ m and the antenna array elements at both

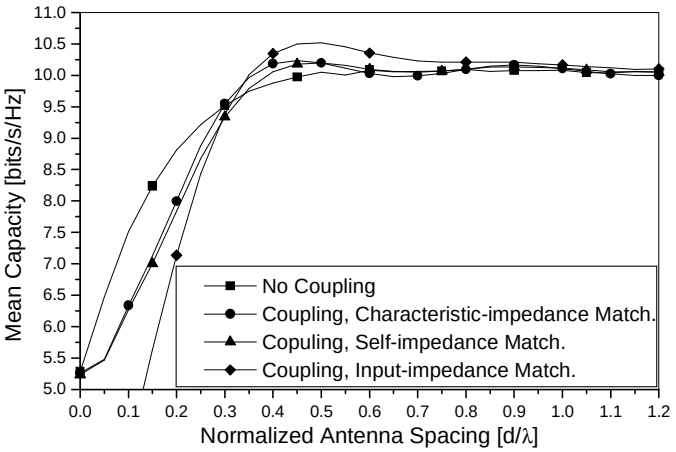

Fig. 4. The mean capacity with and without mutual coupling in USS environments.

vehicles have the azimuth and elevation angles $\theta_T = \theta_R = 0^\circ$ and $\psi_T = \psi_R = 0^\circ$, respectively. The path loss exponent γ is set to 4. Fig. 5 assumes the 3-D non-isotropic radio propagation ($k_T = k_R = 3$, $\beta_{T_m} = \beta_{R_m} = 10^\circ$) in IH environments ($\eta_T = \eta_R = 0.35$, $\eta_{TR} = 0.3$). Note that in IH environments, the single-bounced rays bear more energy than the double-bounced rays [9]. The rest of the parameters in Fig. 5 are chosen as in Fig. 4. The instantaneous capacity is averaged over 5000 channel realizations. Figs. 4 and 5 show

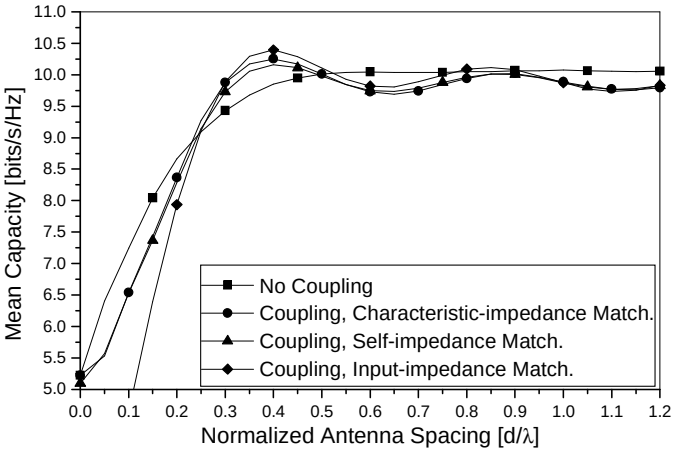

Fig. 5. The mean capacity with and without mutual coupling in IH environments.

that the capacities in USS and IH environments are relatively similar and independent of the propagation environments. The results also show that for the antenna element spacings $0 - 0.3\lambda$, the system with input-impedance matching network provides the smallest capacity, while the capacity of systems with self- and characteristic impedance matching networks are slightly smaller than that of the system without mutual coupling. Furthermore, these results imply that the MIMO V-to-V channel model without mutual coupling overestimates the available capacity and illustrate the importance of incorporating the effect of mutual coupling into propagation models. Note that these results differ from the results obtained for F-to-M channels, where the capacity with mutual coupling is larger than the capacity without mutual coupling for arbitrary antenna spacings [11]. On the other hand, for the antenna element spacings $0.3\lambda - 0.8\lambda$, the results show that all three systems with mutual coupling have similar capacities and outperform the system without mutual coupling. Finally, for the antenna spacings larger than 0.8λ, the capacities of systems with mutual coupling converge to that of the system without mutual coupling.

V. Conclusion

This paper proposed the 3-D propagation model for narrowband MIMO V-to-V multipath fading channels with mutual coupling among both, $\mathrm{T_x}$ and $\mathrm{R_x}$ antennas. This model is used to evaluate the effect of mutual coupling on the $\mathrm{T_x}$ and $\mathrm{R_x}$ antenna patterns and capacity of MIMO V-to-V systems in USS and IH environments.

References

[1] A. S. Akki and F. Haber, "A statistical model for mobile-to-mobile land communication channel," *IEEE Trans. on Veh. Tech.*, vol. 35, pp. 2–10, Feb. 1986.

[2] R. Wang and D. Cox, "Channel modeling for ad hoc mobile wireless networks," *Proc. IEEE VTC'02*, vol. 1, pp. 21–25, Birmingham, AL, May 2002.

[3] C. S. Patel, G. L. Stüber, and T. G. Pratt, "Simulation of Rayleigh-faded mobile-to-mobile communication channels," *IEEE Trans. on Commun.*, vol. 53, pp. 1876–1884, Nov. 2005.

[4] M. Pätzold, B. O. Hogstad, N. Youssef, and D. Kim, "A MIMO mobile-to-mobile channel model: Part I-the reference model," *Proc. IEEE PIMRC'05*, vol. 1, pp. 573–578, Berlin, Germany, Sept. 2005.

[5] B. O. Hogstad, M. Pätzold, N. Youssef, and D. Kim, "A MIMO mobile-to-mobile channel model: Part II-the simulation model," *Proc. IEEE PIMRC'05*, vol. 1, pp. 562–567, Berlin, Germany, Sept. 2005.

[6] A. G. Zajić and G. L. Stüber,"Space-time correlated mobile-to-mobile channels: modeling and simulation," *IEEE Trans. on Veh. Tech.*, vol. 57, pp. 715–726, Mar. 2008.

[7] A. G. Zajić and G. L. Stüber, "Three-dimensional modeling, simulation, and capacity analysis of spacetime correlated mobile-to-mobile channels," *IEEE Trans. on Veh. Tech.*, vol. 57, pp. 2042–2054, July 2008.

[8] A.G. Zajić and G.L. Stüber, "Three-dimensional modeling and simulation of wideband MIMO mobile-to-mobile channels," *IEEE Trans. on Wireless Commun.*, vol. 8, pp. 1260–1275, Mar. 2009.

[9] A. G. Zajić, G. L. Stüber, T. G. Pratt, and S. Nguyen, "Wide-band mimo mobile-to-mobile channels: geometry-based statistical modeling with experimental verification," *IEEE Trans. Veh. Tech.*, vol. 58, pp. 517–534, Feb. 2009.

[10] C. A. Balanis, *Antenna theory: analysis and design.*Wiley, 1997.

[11] J. W. Wallace and M. A. Jensen, "Mutual coupling in MIMO wireless systems: A rigorous network theory analysis," *IEEE Trans. on Wireless Comm.*, vol. 3, pp. 1317–1325, July 2004.

[12] M. K. Özdemir, H. Arslan, and E. Arvas, "On the correlation analysis of antennas in adaptive MIMO systems with 3-D multipath scattering," *Proc. IEEE WCNC'04*, pp. 295–299, Atlanta, GA, Mar. 2004.

[13] R. Janaswamy, "Effect of element mutual coupling on the capacity of fixed length linear arrays," *IEEE Antennas Wireless Propag. Lett.*, vol. 1, pp. 157–160, Aug. 2006.

[14] B. K. Lau, J. B. Andersen, G. Kristensson, and A. F. Molisch, "Impact of matching network on bandwidth of compact antenna arrays," *IEEE Trans. on Antennas and Propagation*, vol. 54, pp. 3225–3238, Nov. 2006.

[15] A. R. Djordjević, M. B. Bazdar, T. K. Sarkar, and R. F. Harrington, *AWAS for Windows: Analysis of Wire Antennas and Scatterers, Software and User's Manual*, Boston: Artech House, 2002.